Three-Dimensional Vacancy Diffusion Analysis Related to Micro Damage of C(T) Specimen for P92 Steel under Creep Condition

Haruhisa Shigeyama[1,*], A. Toshimitsu Yokobori, Jr.[1], Ryuji Sugiura[1], Takashi Matsuzaki[1]

[1] Department of Nanomechanics, Tohoku University, Sendai 980-8579, Japan
* Corresponding author: shigeyama@md.mech.tohoku.ac.jp

Abstract In this study, interrupted creep crack growth tests were conducted using C(T) specimens with side-grooves of P92 steel. After the interrupted tests, to investigate the creep crack growth behavior of P92 steel under the multi-axial stress field, the creep crack growth path of the center of the thickness direction and near the side-groove were observed. From observational results, it was indicated that the creep crack preferentially grew near the side-groove. Additionally, creep crack growth forms were different between the center of the thickness direction and near the side-groove. For the center of the thickness direction, the creep crack growth behavior showed the periodic convexo-concave manner. On the other hand, the creep crack grew in a linear manner near the side-groove. To mechanically clarify the difference of creep crack growth forms, three-dimensional diffusion analysis of vacancies which related to the void formation and crack growth was conducted. From analytical results, vacancies accumulated at the corner of the bottoms of notch and side-groove. This result is in good agreement with the experimental result.

Keywords P92 steel, C(T) specimen, Interrupted test, Creep crack growth, Three-dimensional stress induced vacancy diffusion analysis

1. Introduction

The W-strengthened 9%Cr ferritic heat-resistant steel (ASME code case 2179, ASTM A335 P92) has been developed as a boiler material for the ultra-supercritical power plant. When a component is used in the actual plant, the multi-axial stress field is caused due to the complicated three-dimensional structure. It is known that the ductility of materials decrease with increasing the multi-axial stress and this phenomenon is called “structural brittleness” [1, 2]. The reduction of ductility makes the lifetime-prediction difficult. Therefore, it is important to clarify the creep damage progression behavior of P92 steel under the multi-axial stress field.

It is reported that the initiation and growth of creep voids are accelerated due to the multi-axial stress field [3-6]. Additionally, the initiation and growth of creep voids were caused by the diffusion and accumulation of vacancies. Thus, it is necessary to clarify the diffusion behavior of vacancies under the multi-axial stress field. Actually, some authors proposed the numerical analytical method of two-dimensional stress induced vacancy diffusion [7-10].

In this study, interrupted creep crack growth (CCG) tests were conducted using C(T) specimens with side-grooves of P92 steel. After the interrupted tests, to investigate the CCG behavior of P92 steel under the multi-axial stress field, the CCG path of the center of the thickness direction and near the side-groove were observed. Then, three-dimensional stress induced vacancy diffusion analysis was conducted to clarify the diffusion behavior of vacancies for C(T) specimen with side-grooves.

2. Experimental Procedures

2.1. Material and Specimen

The material used is P92 steel. The chemical composition of P92 steel is shown in Table 1. The specimen used is a C(T) specimen with side-grooves of 25% of specimen thickness. The geometry and size of the C(T) specimen is shown in Fig. 1.

Table 1. Chemical composition of P92 steel in wt.%

C	Si	Mn	P	S	Cr	Mo	W	Nb	V	N	B
0.085	0.26	0.49	0.006	0.0012	8.85	0.50	1.80	0.06	0.20	0.0510	0.0030

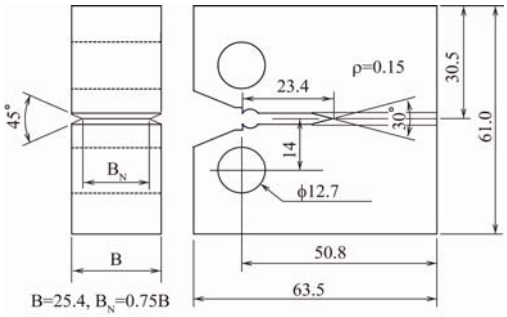

Figure 1. The geometry and size of a C(T) specimen (Unit: mm)

2.2. CCG Tests Procedures and Experimental Conditions

The interrupted CCG tests were conducted by lever-arm high temperature creep testing machine (Type RT-30) manufactured by TOSHIN KOGYO. The creep crack length was measured by direct current potential drop (DCPD) method [11, 12]. Load line displacement (LLD) was measured by displacement sensing bars and linear gauges. A schematic illustration of measurement methods of creep crack length and LLD is shown in Fig. 2. The interrupted CCG tests were carried out under the conditions of 600 °C and initial stress intensity factor K_{in} = 42 MPam$^{1/2}$. These tests were interrupted at different times, as shown in Table 2.

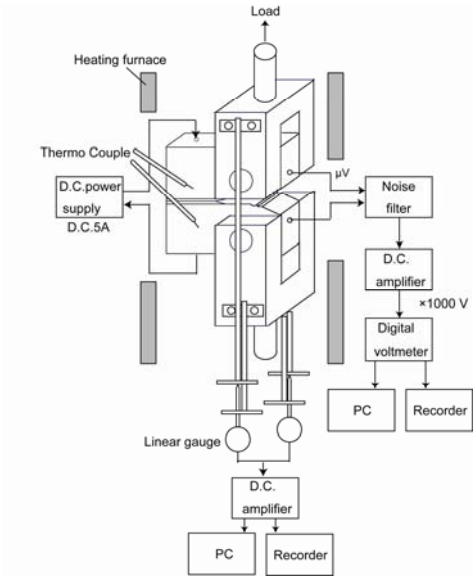

Figure 2. Measurement methods of creep crack length and LLD

Table 2. Experimental conditions of interrupted CCG tests

Temperature [°C]	Initial stress intensity factor K_{in} [MPam$^{1/2}$]	Interrupted time [hr]	Creep life fraction t/t_f
600	42	52.5	0.17
		150	0.50
		226	0.75
		301	0.99

3. Three-dimensional Vacancy Diffusion Analysis

The numerical analytical method of stress induced particle diffusion was proposed by Yokobori, *et al.* [13-15]. In this method, the stress distribution is calculated by finite element analysis (FEA) and stress induced particle migration is calculated by finite difference analysis (FDA). This analytical method was applied to the problems of hydrogen embrittlement [13, 14, 16], stressmigration and electromigration of LSI interconnect [8-10, 17] and high-temperature creep of heat-resistant steels [7]. All of these analyses were conducted in two dimensions. However, the actual plant has a complicated three-dimensional structure. Therefore, to apply this analytical method to the actual components, it is important to conduct the three-dimensional vacancy diffusion analysis. Thus, in this paper, the numerical analytical method of three-dimensional vacancy diffusion was developed and applied to the high-temperature creep of C(T) specimen.

3.1. Basic Equation of Vacancy Diffusion

Based on a multiplication concept [13-15], the basic equation of three-dimensional vacancy diffusion is given by Eq. (1).

$$\begin{aligned}\frac{\partial C}{\partial t} &= \alpha_1 D\left(\frac{\partial^2 C}{\partial x^2}+\frac{\partial^2 C}{\partial y^2}+\frac{\partial^2 C}{\partial z^2}\right)-\alpha_2 D\frac{\Delta V}{RT}\left(\frac{\partial C}{\partial x}\frac{\partial \sigma_p}{\partial x}+\frac{\partial C}{\partial y}\frac{\partial \sigma_p}{\partial y}+\frac{\partial C}{\partial z}\frac{\partial \sigma_p}{\partial z}\right)\\ &\quad -\alpha_3 D\frac{\Delta V}{RT}C\left(\frac{\partial^2 \sigma_p}{\partial x^2}+\frac{\partial^2 \sigma_p}{\partial y^2}+\frac{\partial^2 \sigma_p}{\partial z^2}\right)\end{aligned} \tag{1}$$

where C is concentration of vacancies, t is time, D is the self diffusion coefficient of P92 steel, ΔV is a volume change due to accommodation of a vacancy, R is gas constant, T is absolute temperature, σ_p is hydrostatic stress, and α_i are the weight coefficients. The self diffusion coefficient D is given by Eq. (2).

$$D = D_0 \exp\left(-\frac{Q}{RT}\right) \tag{2}$$

where D_0 and Q are diffusion constant and activation energy of P92 steel, respectively.

3.2. Analytical Methods and Conditions

Distribution of hydrostatic stress for C(T) specimen was calculated by three-dimensional FEA. This analysis was performed by MSC Marc / MSC Marc Mentat ver. 2009 (Cyber Science Center, Tohoku University). A finite element model of C(T) specimen is shown in Fig. 3. Due to symmetry, only one quarter of the specimen is meshed. The material properties of P92 steel used in the FEA were shown in Table 3. Work hardening due to the plastic deformation is given by Eq. (3).

$$\bar{\sigma} = c\bar{\varepsilon}_p \tag{3}$$

where, $\bar{\sigma}$ is equivalent (Mises) stress, and $\bar{\varepsilon}_p$ is equivalent plastic strain.

The distributions of vacancy concentration were obtained by solving Eq. (1) using three -dimensional FDA. Figure 4 shows a model of three-dimensional vacancy diffusion analysis. To match the finite difference lattice and finite element mesh, unequally-spaced finite difference lattice was used in the FDA. Equation (1) was converted into the non-dimensional equation using the non-dimensional values given by Eq. (4).

$$x^+ = \frac{x}{a},\quad y^+ = \frac{y}{a},\quad z^+ = \frac{z}{a},\quad C^+ = \frac{C}{C_0},\quad t^+ = D_0\frac{t}{a^2},\quad D^+ = \frac{D}{D_0} = \exp\left(-\frac{Q}{RT}\right) \tag{4}$$

The non-dimensional equation is discretized by the Crank−Nicolson implicit method and Eq. (5)

was obtained.

$$\begin{aligned}
&A(x,y,z)C^{+\,n+1}_{i+1,j,k} + \left(B(x,y,z)-1\right)C^{+\,n+1}_{i,j,k} + E(x,y,z)C^{+\,n+1}_{i-1,j,k} + F(x,y,z)C^{+\,n+1}_{i,j+1,k} \\
&+ G(x,y,z)C^{+\,n+1}_{i,j-1,k} + H(x,y,z)C^{+\,n+1}_{i,j,k+1} + I(x,y,z)C^{+\,n+1}_{i,j,k-1} \\
&= -A(x,y,z)C^{+\,n}_{i+1,j,k} - \left(B(x,y,z)+1\right)C^{+\,n}_{i,j,k} - E(x,y,z)C^{+\,n}_{i-1,j,k} - F(x,y,z)C^{+\,n}_{i,j+1,k} \\
&- G(x,y,z)C^{+\,n}_{i,j-1,k} - H(x,y,z)C^{+\,n}_{i,j,k+1} - I(x,y,z)C^{+\,n}_{i,j,k-1}
\end{aligned} \tag{5}$$

where,

$$A(x,y,z) = \frac{\Delta t^+}{\Delta x_i^+\left(\Delta x_{i-1}^+ + \Delta x_i^+\right)}\left(\alpha_1 D^+ - \frac{\alpha_2 D^+ \Delta V \Delta x_{i-1}^+}{2RT}\frac{\partial \sigma_p}{\partial x^+}\right)$$

$$\begin{aligned}
B(x,y,z) = &-\alpha_1 D^+ \Delta t^+\left(\frac{1}{\Delta x_{i-1}^+ \Delta x_i^+} + \frac{1}{\Delta y_{j-1}^+ \Delta y_j^+} + \frac{1}{\Delta z_{k-1}^+ \Delta z_k^+}\right) \\
&- \frac{\alpha_2 D^+ \Delta V \Delta t^+}{2RT}\left(\frac{\Delta x_i^+ - \Delta x_{i-1}^+}{\Delta x_{i-1}^+ \Delta x_i^+}\frac{\partial \sigma_p}{\partial x^+} + \frac{\Delta y_j^+ - \Delta y_{j-1}^+}{\Delta y_{j-1}^+ \Delta y_j^+}\frac{\partial \sigma_p}{\partial y^+} + \frac{\Delta z_k^+ - \Delta z_{k-1}^+}{\Delta z_{k-1}^+ \Delta z_k^+}\frac{\partial \sigma_p}{\partial z^+}\right) \\
&- \frac{\alpha_3 D^+ \Delta V \Delta t^+}{2RT}\left(\frac{\partial^2 \sigma_p}{\partial x^{+\,2}} + \frac{\partial^2 \sigma_p}{\partial y^{+\,2}} + \frac{\partial^2 \sigma_p}{\partial z^{+\,2}}\right)
\end{aligned}$$

$$E(x,y,z) = \frac{\Delta t^+}{\Delta x_{i-1}^+\left(\Delta x_{i-1}^+ + \Delta x_i^+\right)}\left(\alpha_1 D^+ + \frac{\alpha_2 D^+ \Delta V \Delta x_i^+}{2RT}\frac{\partial \sigma_p}{\partial x^+}\right)$$

$$F(x,y,z) = \frac{\Delta t^+}{\Delta y_j^+\left(\Delta y_{j-1}^+ + \Delta y_j^+\right)}\left(\alpha_1 D^+ - \frac{\alpha_2 D^+ \Delta V \Delta y_{j-1}^+}{2RT}\frac{\partial \sigma_p}{\partial y^+}\right)$$

$$G(x,y,z) = \frac{\Delta t^+}{\Delta y_{j-1}^+\left(\Delta y_{j-1}^+ + \Delta y_j^+\right)}\left(\alpha_1 D^+ + \frac{\alpha_2 D^+ \Delta V \Delta y_j^+}{2RT}\frac{\partial \sigma_p}{\partial y^+}\right)$$

$$H(x,y,z) = \frac{\Delta t^+}{\Delta z_k^+\left(\Delta z_{k-1}^+ + \Delta z_k^+\right)}\left(\alpha_1 D^+ - \frac{\alpha_2 D^+ \Delta V \Delta z_{k-1}^+}{2RT}\frac{\partial \sigma_p}{\partial z^+}\right)$$

$$I(x,y,z) = \frac{\Delta t^+}{\Delta z_{k-1}^+\left(\Delta z_{k-1}^+ + \Delta z_k^+\right)}\left(\alpha_1 D^+ + \frac{\alpha_2 D^+ \Delta V \Delta z_k^+}{2RT}\frac{\partial \sigma_p}{\partial z^+}\right) \tag{6}$$

$$x^+ = \sum_{l=1}^{i-1}\Delta x_l^+, \quad y^+ = \sum_{m=1}^{j-1}\Delta y_m^+, \quad z^+ = \sum_{n=1}^{k-1}\Delta z_n^+$$

The obtained simultaneous equations were solved by the successive over relaxation (SOR) method. The material properties of P92 steel used in the FDA were shown in Table 4. It is known that vacancies were generated with the progress of the plastic deformation [18]. Therefore, distribution of initial vacancy concentration C_0 was set based on the distribution of equivalent plastic strain obtained by 3D-FEA as follows.

$$C_0 = 1.0 + b\bar{\varepsilon}_p \tag{7}$$

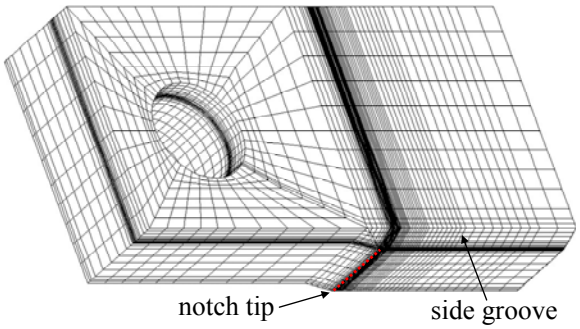

Figure 3. Three-dimensional finite element model (1/4 C(T) specimen)

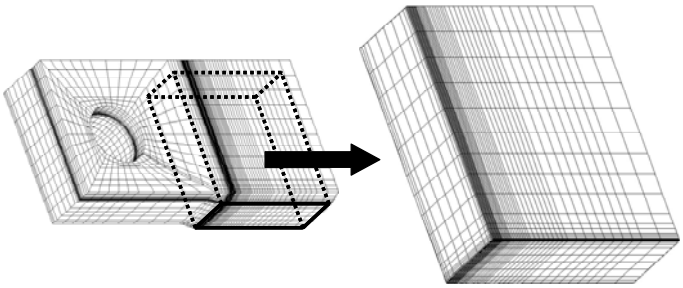

Figure 4. Three-dimensional finite difference model

Table 3. Material properties of P92 steel used in the FEA (600°C)

E [GPa]	ν	σ_{ys} [MPa]	c [MPa]
164	0.3	380	16400

Table 4. Material properties of P92 steel used in the FDA

R [J/Kmol]	ΔV [mm³/mol]	T [K]	Q [J/mol]	D_0 [mm²/sec]	C_0^e	b	α_1	α_2	α_3
8.31	2.00×10^3	873	2.00×10^5	3.72×10^1	1.00	50	10000	2000	10

4. Results and Discussions

4.1. Characteristics of CCG and LLD

The relationship between creep crack length Δa measured by DCPD method and creep life fraction t/t_f is shown in Fig. 5. The relationship between LLD $\Delta\delta$ and creep life fraction t/t_f is shown in Fig. 6. Where, t and t_f are the current time of load application and the life of CCG. From Fig. 5, creep crack was gradually accelerated from about 20% of CCG life. And the characteristic of CCG did not show the steady-state CCG rate region. On the other hand, the characteristic of LLD showed the steady-state creep deformation and it occupied approximately 50% of total life as shown in Fig. 6.

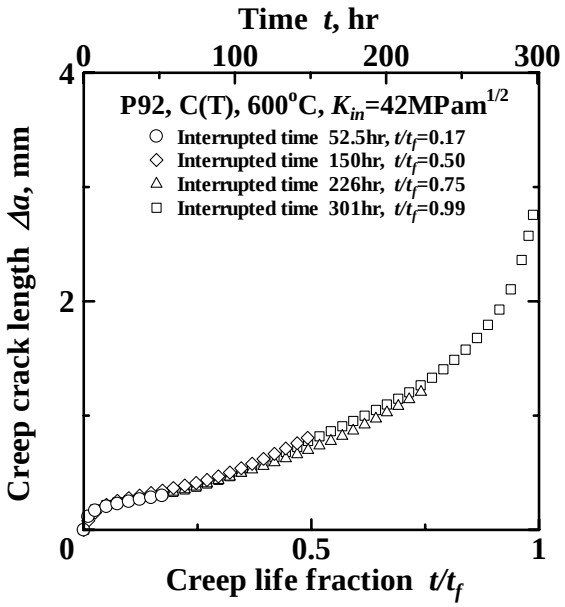

Figure 5. Characteristic of CCG

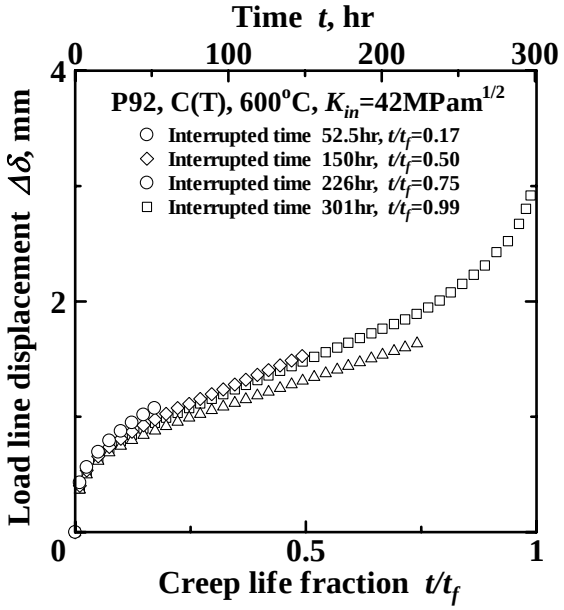

Figure 6. Characteristic of LLD

4.2. Observations of CCG Path

To investigate the three-dimensional CCG behavior for C(T) specimen of P92 steel, the CCG path at the center of the thickness direction (hereinafter referred to as "center") and near the side-groove (hereinafter referred to as "side") were observed using laser microscope. The observational results of the center and the side are shown in Fig. 7 and Fig. 8, respectively. From Fig. 7, the CCG behavior showed the periodic convexo-concave manner at the center. This crack path is called "fracture unit area (FA) cracking" [19-21]. On the other hand, the creep crack grew in a linear manner at the side as shown in Fig. 8.

Creep crack length of each interrupted times were measured. At 52.5h (t/t_f = 0.17), the creep crack did not initiate both at the center and at the side. After the middle of total life (t/t_f > 0.50), the creep crack has already initiated both at the center and at the side. And the creep crack length of the side was longer than that of the center. This tendency became marked at 226h (t/t_f = 0.75). This result indicates that the creep crack was preferential growth at the side from 50% to 75% of total life and accelerated at the center after 75% of total life. Therefore, it seems that the creep crack of C(T) specimen with side-grooves grew as shown in Fig. 9. The characteristic of CCG without the steady-state CCG rate region is thought to be due to the preferential CCG at the side.

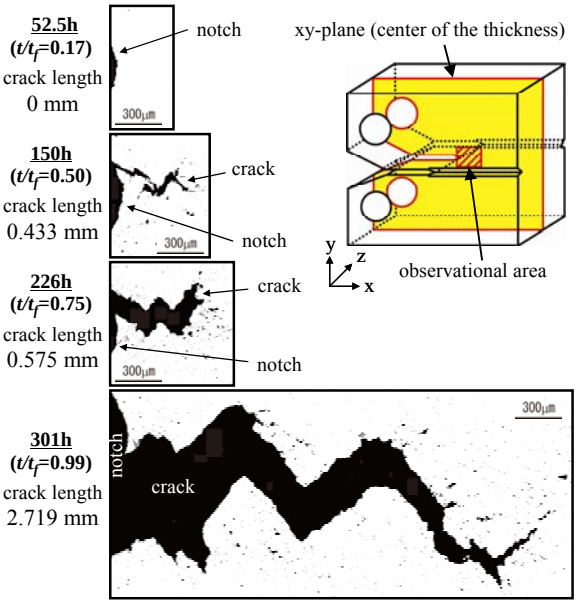

Figure 7. CCG path of center

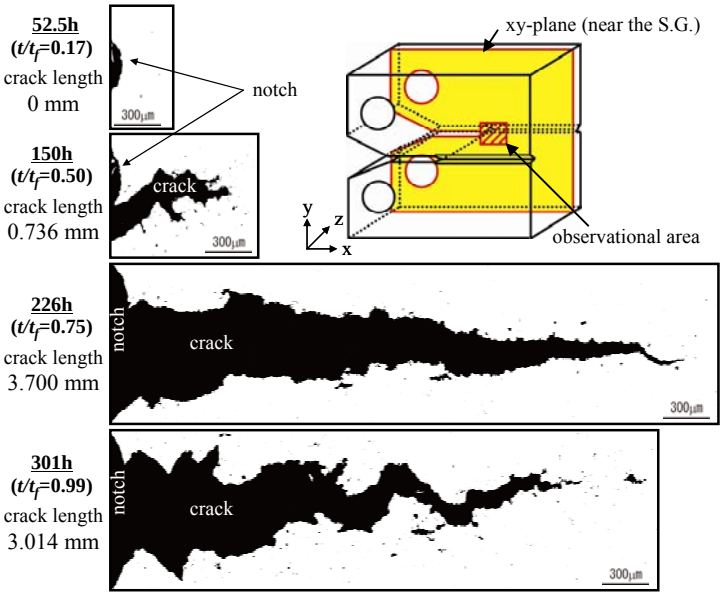

Figure 8. CCG path of side

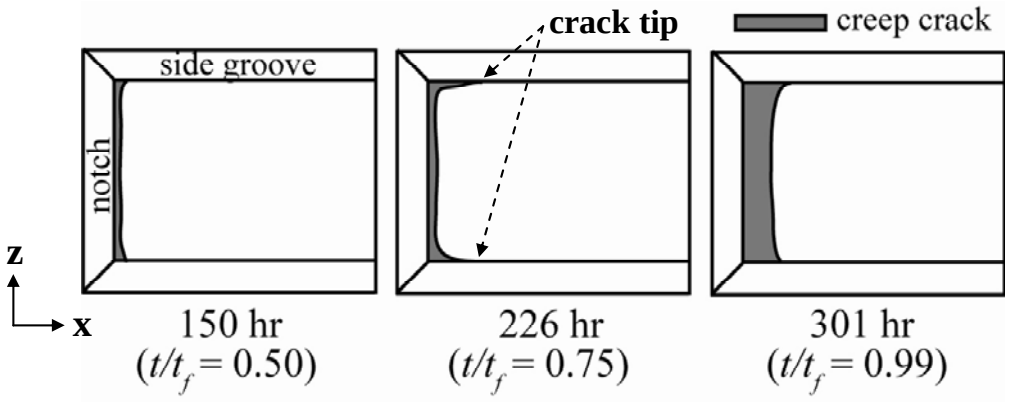

Figure 9. Schematic illustrations of CCG process on the xz-plane

4.3. Analytical Results

Figure 10 (a) and (b) represent the distributions of vacancy concentration at 0h (initial) and 100h in a shaded area shown in Fig. 11, respectively. From these figures, vacancies remarkably accumulated at the corner of the bottoms of notch and side-groove. And vacancies also accumulated at the bottom of side-groove near the notch tip. These results are in good agreement with the experimental result of the preferential CCG at the side. Figure 12 (a)-(c) show the distributions of vacancy concentration along line segment oa, bc and ob shown in Fig. 11, respectively. From Fig. 12 (b), the vacancy concentration at the bottom of side-groove increased within about 3 mm from the notch tip and this length correspond to the creep crack length of 226h and 301h at the side. These results indicate that the creep crack preferentially grows in the region of high vacancy concentration. Therefore, it seems that the three-dimensional vacancy diffusion analysis is useful to predict the behavior of creep damage such as creep voids and cracks.
From the experimental results, it was clarified that the creep crack of C(T) specimen with side-grooves of 25% of specimen thickness preferentially grew near the side-groove. On the other hand, the creep crack of C(T) specimen without side-grooves preferentially grows at the center and this is crack tunneling. Three-dimensional vacancy diffusion analysis enables us to predict the most appropriate depth of side-grooves which cause the uniform creep crack growth in the thickness direction.

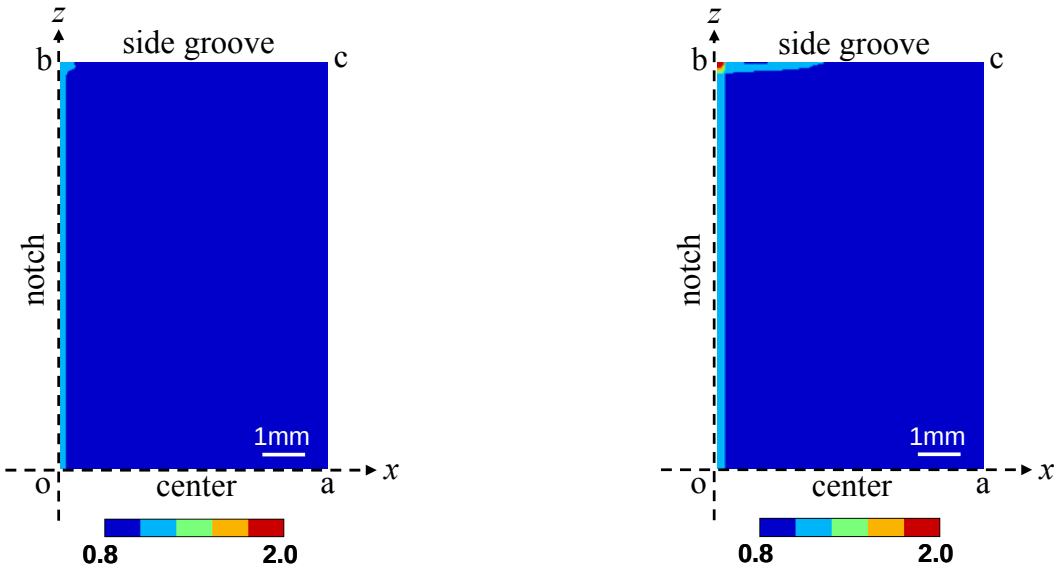

(a) 0h (initial) (b) 100h

Figure 10. Distributions of vacancy concentration at a shaded area shown in Fig. 10

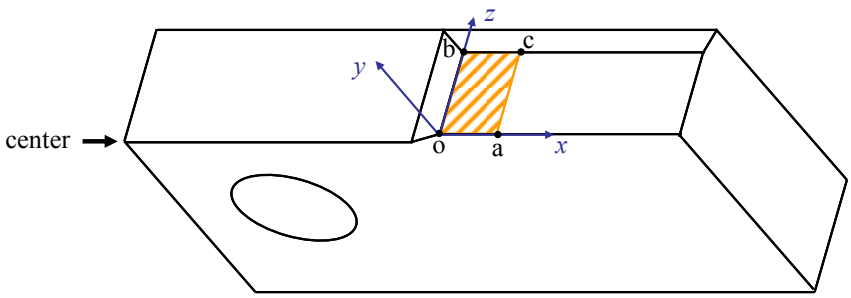

Figure 11. A Schematic illustration of 1/4 C(T) specimen

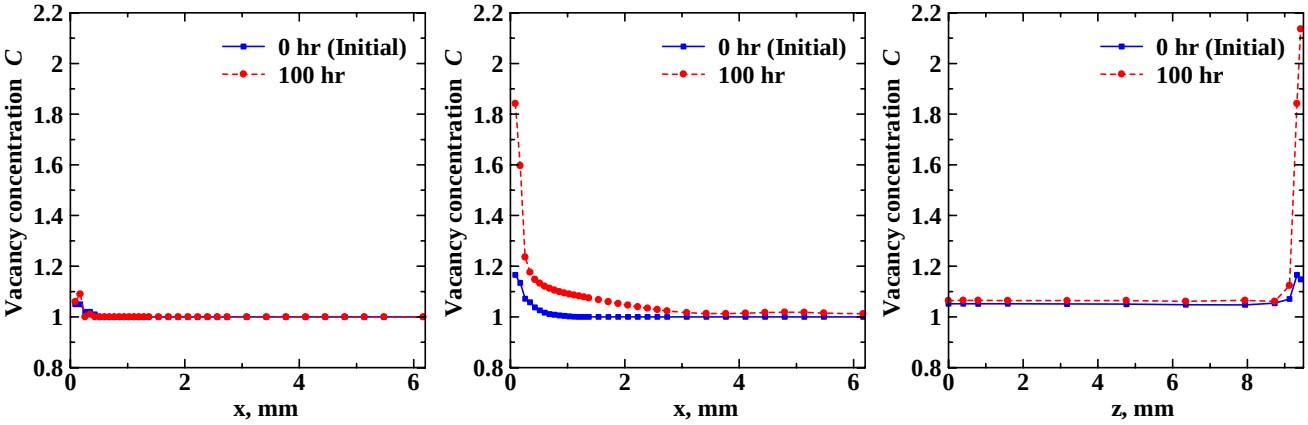

(a) Line segment oa (center) (b) Line segment bc (side) (c) Line segment ob (notch)

Figure 12. Distributions of vacancy concentration along each line segment

5. Conclusions

Interrupted CCG tests were conducted using C(T) specimens with side-grooves of P92 steel. Then, the creep crack growth path of each interrupted specimen was observed and the creep crack growth behavior of P92 steel was investigated. Furthermore, the three-dimensional vacancy diffusion analysis was conducted to clarify the three-dimensional diffusion behavior of vacancies which related to the void formation and crack growth. Following results were obtained:

(1) The creep crack growth forms were different between the center of the thickness direction and near the side-groove. For the center of the thickness direction, the creep crack growth behavior showed the periodic convexo-concave manner. On the other hand, the creep crack grew in a linear manner near the side-groove.

(2) The creep crack of C(T) specimen with side-grooves of 25% of specimen thickness preferentially grew near the side-groove.

(3) Vacancies remarkably accumulated at the corner of the bottoms of notch and side-groove. The vacancy concentration at the bottom of side-groove increased within about 3 mm from the notch tip and this length correspond to the creep crack length of 226h and 301h near the side-groove.

(4) The three-dimensional vacancy diffusion analysis is useful to predict the behavior of creep damage such as creep voids and cracks.

Acknowledgements

This work was partly supported by the Japan Society for the Promotion of Science Research Fellow 24.2235.

References

[1] A.T. Yokobori, Jr., R. Sugiura, M. Tabuchi, A. Fuji, T. Adachi, T. Yokobori, The effect of multi-axial stress component on creep crack growth rate concerning structural brittleness, Proc ICF 11 (2005) CD-ROM.

[2] R. Sugiura, A.T. Yokobori, Jr., M. Tabuchi, A. Fuji, T. Adachi, Characterization of structural embrittlement of creep crack growth for W-added 12%Cr ferritic heat-resistant steel related to the multi axial stress, Trans of ASME, J Eng Mater Technol, 131 (2009) 011004 1-9.

[3] K. Kimura, K. Fujiyama, R. Ishi, K. Saito, Estimation of Creep Damage for the Components of Mod. 9Cr-1Mo Steel: (2nd Report, Creep Damage Assessment for Welded Joint by Means of Void Observation), Trans Jpn Soc Mech Eng, A 66(647) (2000) 1411-1418 (in Japanese).

[4] T. Watanabe, M. Yamazaki, H. Hongo, M. Tabuchi, T. Tanabe, Relationship between Type IV

Fracture and Microstructure on 9Cr-1Mo-V-Nb Steel Welded Joint Creep-ruptured after Long Term, Tetsu-to-Hagane, 90(4) (2004) 206-212 (in Japanese).
[5] T. Ogata, T. Sakai, M. Yaguchi, Damage characterization of a P91 steel weldment under uniaxial and multiaxial creep, Mater Sci Eng A, 510−511 (2009) 238−243.
[6] H. Hongo, M. Tabuchi, T. Watanabe, Type IV Creep Damage Behavior in Gr.91 Steel Welded Joints, Metall Mater Trans A, 43A (2012) 1163-1173.
[7] A.T. Yokobori, Jr., K. Abe, H. Tsukidate, T. Ohmi, R. Sugiura, H. Ishikawa, Micro mechanics based on vacancy diffusion coupled with damage mechanics related to creep deformation and prediction of creep fracture life, Mater High Temp, 28(2) (2011) 126-136.
[8] S. Nakajima, T. Nemoto, A.T. Yokobori, Jr., Lifetime prediction of stress induced voiding failure by novel numerical analysis in Cu interconnects with an ultra low-k dielectric, Proc AMC, (2009) 751-755.
[9] H. Shigeyama, T. Nemoto, A.T. Yokobori, Jr., Prediction of stress induced voiding reliability in Cu damascene interconnect by computer aided vacancy migration analysis, Jpn J Appl Phys, 50 (2011) 05EA05 1-6.
[10] H. Shigeyama, A.T. Yokobori, Jr., T. Ohmi, T. Nemoto, Analysis of stress induced voiding using by finite element analysis coupled with finite difference analysis, Defect Diffus Forum, 326-328 (2012) 632-640.
[11] H.H. Johnson, Calibrating the electric potential method for studying slow crack growth, Mater Res Stand, 5 (1965) 442-445.
[12] K.H. Schwalbe, D. Hellmann, Application of the electrical potential method to crack length measurements using Johnson's formula, J Test Eval, 9(3) (1981) 218-221.
[13] A.T. Yokobori, Jr., T. Nemoto, K. Satoh, T. Yamada, Numerical analysis on hydrogen diffusion and concentration in solid with emission around the crack tip, Eng Fract Mech, 55(1) (1996) 47-60.
[14] A.T. Yokobori, Jr., Y. Chinda, T. Nemoto, K. Sato, T. Yamada, The characteristics of hydrogen diffusion and concentration around a crack tip concerned with hydrogen embrittlement, Corro Sci, 44(3) (2002) 407-424.
[15] A.T. Yokobori, Jr., T. Ohmi, T. Murakawa, T. Nemoto, T. Uesugi R. Sugiura, The application of the analysis of potential driven particle diffusion to the strength of materials, Strength, Fract Complex, 7 (2011) 215-233.
[16] A.T. Yokobori, Jr., T. Uesugi, M. Sendoh, M. Shibata, The effect of stress wave form on corrosion fatigue crack growth rate on the basis of hydrogen diffusion theory, Strength, Fract Complex, 1(4) (2003) 187-204.
[17] T. Nemoto, A.T. Yokobori, Jr., T. Murakawa, H. Miura, Numerical Analysis of Vacancy Transport by Residual Stress in Electromigration on LSI Interconnects, Jpn J Appl Phys, 49 (2010) 024301 1-7.
[18] T. Yokobori, Strength of Materials, Iwanami, Tokyo, 1964.
[19] A.T. Yokobori Jr., S. Takmori, T. Yokobori, Y. Hasegawa, K. Kubota, K. Hidaka, Mechanical Behavior and Strengthening Mechanism of W containing 9-12% Cr Steels under Creep Conditon for a Cracked Specimen, Key Eng Mater, 171-174 (2000) 131-138.
[20] R. Sugiura, A.T. Yokobori Jr., S. Takamori, M. Tabuchi, A. Fuji, M. Yoda, K. Kobayashi, T. Yokobori, Effects of Alloying Additions and Material Microstructure on the Accuracy of the Predictive Law of Creep Crack Growth for W-Strengthened 9-12%Cr Ferritic Heat-Resistant Steel, Mater Trans, 48(11) (2007) 2928-2936.
[21] Y. Nagumo, A.T. Yokobori, Jr., R. Sugiura, T. Matsuzaki, The occurrence mechanism of periodicity of creep crack path for P92, J ASTM Int, 8(8) (2011) 1-11.